Podugu, N., Mishra, S., Wiersberg, T., Roy, S. (2019): Chemical and Noble Gas Isotope Compositions of Formation Gases from a 3 km Deep Scientific Borehole in the Koyna Seismogenic Zone, Western India. - *Geofluids*, *2019*, pp. 1—16.

DOI: http://doi.org/10.1155/2019/1078942

Hindawi
Geofluids
Volume 2019, Article ID 1078942, 16 pages
https://doi.org/10.1155/2019/1078942

Research Article

Chemical and Noble Gas Isotope Compositions of Formation Gases from a 3 km Deep Scientific Borehole in the Koyna Seismogenic Zone, Western India

Nagaraju Podugu,[1] **Satrughna Mishra**,[1] **Thomas Wiersberg**,[2] **and Sukanta Roy**[1]

[1]*Ministry of Earth Sciences, Borehole Geophysics Research Laboratory, Karad 415 114, India*
[2]*GFZ German Research Centre for Geosciences, Telegrafenberg, 14473 Potsdam, Germany*

Correspondence should be addressed to Nagaraju Podugu; nagarajupodugu@yahoo.com

Received 14 March 2019; Revised 2 June 2019; Accepted 16 August 2019; Published 17 September 2019

Academic Editor: Francesco Italiano

A 3 km deep research borehole KFD1 was drilled in the Koyna reservoir-triggered seismicity region, Western India, between December 2016 and May 2017. The 1967 *M* 6.3 Koyna earthquake had generated a NNE-SSW trending surface fissure zone in the Nanel-Donichawadi-Kadoli sector. KFD1 is located ~5 km south of Kadoli along the trend of the Donichawadi fault zone. Online gas monitoring was carried out during drilling of KFD1 from 1315 m to 2831 m depth to sample and study the composition of crustal gases. Formation gases CO_2, CH_4, H_2, and He were only observed during water flushing of ~100 m intervals following coring runs. Laboratory analyses of gas samples collected between 1737 m and 2831 m depth revealed concentrations of up to 1200 ppmv CO_2, 186 ppmv CH_4, 139 ppmv H_2, and 12.8 ppmv He. Zones enriched in gases are mostly below the 2100 m depth with significant He enhancement ranging from 4.6 to 7.6 ppmv above the atmospheric value. The He-rich zones correlate well with the zones of anomalous physical and mechanical properties identified from geophysical logs and are characterized by high fracture density as revealed from borehole images, indicating that the borehole punctured multiple fracture zones. The helium concentrations are consistent with those previously observed over the surface fissures near Kadoli, suggesting a southward extension of the Donichawadi fault zone up to the KFD1 site and confirming that the fault zone is permeable even after 50 years of the 1967 Koyna earthquake. $^3He/^4He$ ratios of eleven gas samples fall between 0.426 ± 0.022 and 0.912 ± 0.059 Ra, with $^4He/^{20}Ne$ values between 0.3449 ± 0.0091 and 0.751 ± 0.020. Air-corrected helium isotope ratios indicate that helium is a mixture of atmospheric and crustal radiogenic components but no mantle contribution within 2σ analytical uncertainties.

1. Introduction

It is known that fluids are responsible for various processes occurring at seismogenic depths of active fault zones [1], but if and how fluid overpressure is linked with these processes, the origin and magnitude of fluid overpressure, and the role of fluid pressures in controlling the strength of fault zones are still under debate [2–4]. Fluid migration and fluid-rock interaction play a role in metamorphic reactions, melting and crystallization processes, mass and heat transport, and the deep biosphere and rheological behaviour of rocks in the Earth's crust.

Deep drilling provides an opportunity to examine pristine fluids from the subsurface. In many cases of deep drilling, drilling mud is circulated to stabilize the borehole, to cool the drill bit, and to drag out the rock chips (cuttings) from the borehole. Formation fluids and gases return to the surface with the drilling mud, where they can be monitored and sampled. Mud gas logging is a common technique in the oil and gas industry to evaluate hydrocarbon reservoir rocks and for safety reasons. In the past few decades, online mud gas monitoring and sampling has been carried out in association with several scientific deep drilling programmes in crystalline rocks to obtain information on crustal gases

[5–7]. Hydrocarbons, He, Rn, CO_2, H_2S, and H_2 are usually enriched in subsurface formation fluids relative to the atmosphere, which therefore make these gases suitable for detection of fluid-bearing horizons including shear zones, open fractures, and other zones with enhanced permeability. Also, a number of studies aimed at detecting geochemical precursors of earthquakes have been carried out as there are strong evidences of preferential degassing at active fault zones [8, 9]. Temporal changes in Rn, He, CO_2, N_2, and CH_4 have been recognized as potential tracers of fault systems [10–17]. However, interpretation in terms of the source of the leaking gas is not straightforward as thermal, radiogenic, and geodynamic processes may be involved in degassing at active faults resulting in a complex pattern of degassing from the crust both in space and time [18].

The continuous fluid analysis during drilling of the KTB (German Continental Deep Drilling Program) boreholes led to determining the composition of gases dissolved in drilling fluid and identifying several fluid flow zones with enhanced gas concentrations above the atmospheric abundances [7, 19]. Subsequently, online monitoring of fluids and gases from circulating drilling mud has been successfully conducted in several scientific drilling projects in crystalline and sedimentary strata with a focus on fault zones, e.g., the San Andreas Fault Observatory at Depth (SAFOD) [7, 20–22], the Wenchuan Fault Zone drilling project [23], and the Nankai Trough Seismogenic Zone Experiment (NanTroSEIZE) [24–26]. Online gas monitoring during drilling through fault zones provides information on the origin and spatial distribution of formation gases at seismogenic depths, gas migration, and the fault zone permeability architecture.

The Koyna region, situated in western India, is a well-known site of reservoir-triggered seismicity (RTS), where triggered earthquakes have been occurring in a restricted area of $30 \times 20\,km^2$ since the impoundment of the Koyna reservoir in 1962 [27–34]. There were no earthquakes reported in the Koyna region prior to impoundment of the reservoir within 50 km of the Koyna dam, but the seismic activity started in the months following the impoundment and increased gradually during the next few years culminating in the M~6.3 Koyna earthquake of December 10, 1967 [29, 35]. The RTS was further enhanced by impoundment of the nearby located Warna reservoir in 1985 [36]. Besides the largest triggered earthquake of M~6.3, the region has experienced 22 earthquakes of $M \geq 5$, about 200 earthquakes of $M > 4$, and several thousand smaller earthquakes in the past 55 years. The region continues to be active with recurrent, low magnitude earthquakes. A strong correlation between earthquake occurrences and the annual loading and unloading cycles of the Koyna and Warna reservoirs has been established from observations during the past few decades [29, 34, 37]. However, a model to comprehend the genesis of reservoir-triggered earthquakes has remained elusive likely due to lack of direct observations from the near-field of earthquakes. A major research programme involving scientific deep drilling investigations in the Koyna seismogenic zone was taken up in the year 2012 to improve our understanding of the mechanism of triggered earthquakes in the region through near-field observations. As part of this research initiative, a 3 km deep pilot borehole KFD1 was drilled between December 2016 and May 2017 at Gothane (17°17′57″N, 73°44′19″E), ~10 km SE of Koyna dam (Figure 1). The ground elevation with respect to the mean sea level is 930 m. The pilot hole drilling provided valuable base information for the proposed main borehole to deploy a deep fault zone observatory at ~5 km depth [38, 39].

The pilot hole site is located in close proximity of the Donichawadi fissure zone, the surface manifestation of the 1967 M 6.3 Koyna earthquake (Figure 1(a)). Although ground fissures and cracks were identified at many localities in the region, a regular pattern and continuity of the fissures was evident over a length of 4 km in the Nanel-Donichawadi-Kadoli sector [40]. A soil-helium survey conducted during 1996-1997 across the fissure zone, 5 km north of the KFD1 drill site, showed helium anomalies up to 7 ppm above atmospheric abundance of 5.24 ppm even 30 years after the 1967 earthquake, signifying the activity of the Donichawadi fissure zone through which formation gases are escaping [41] (Figure 1(b)). Along the same alignment of the Donichawadi fissure zone, small cracks were seen in Randiv village, 12 km south-west of Kadoli [40]. Sathe et al. [42] suggested that this fissure zone extends from Baje to Randiv via Donichawadi and Kadoli, which was later supported by Talwani [31] (Figure 1(a)). However, the continuity of the fissures from Donichawadi to Randiv did not gain support from the detailed examination of hill slopes between these two locations [40]. Therefore, it is not clear whether the Donichawadi fault extends further to the south of Kadoli. On the other hand, the trend of the fissure zone is consistent with the seismic activity in the Koyna region during the past few decades [34]. As the Koyna pilot hole site is located close to the Donichawadi fissure zone, we consider that investigations in KFD1would shed new light on the presence of the active fault zone in the area and the southward extension of the Donichawadi fissure zone.

In the present study, we have carried out online gas monitoring during KFD1 mud drilling and, for the first time, also during air hammer drilling. Eleven gas samples were collected during water flushing after core runs for off-site noble gas isotope studies. The data from online gas analysis (OLGA) and helium isotope data from off-line gas samples are discussed in the context of abundance and composition of gases present in the pilot borehole KFD1, detection of potential fluid-bearing horizons and shear/fracture zones, and confirmation of possible southward extension of the still active Donichawadi fissure zone.

2. Methods

2.1. KFD1 Drilling Operations. Drilling of the Koyna pilot hole KFD1 was mainly done using the air hammer technique except at a few depths where fluid loss or water ingress zones were encountered and at depths where coring was done, in which mud rotary drilling was performed. KFD1 was drilled in three phases. During phase I (December 20, 2016, to January 8, 2017), the borehole was drilled from the surface to 502 m followed by casing and cementation. During phase II (January 11 to March 12, 2017), the borehole penetrated

the basalt-granite intersection at 1251 m and reached a depth of 1503 m, where geophysical logging from 500 m to 1500 m was conducted in the open hole before the borehole was cased and cemented. Finally, during phase III (March 17 to June 11, 2017), the borehole reached the final depth of 3014 m. Cores were obtained using a 9 m long core barrel at intermittent depths starting from 1679 m to 2912 m during eight coring runs. The borehole passed through the base of the Deccan basalt column at 1251 m and continued 1763 m in the underlying granitic basement. All depths are referenced to the kelly bushing, which was located at 3.5 m elevation with respect to ground level. The basement rocks, comprised mainly of cratonic (tonalite-trondhjemite-granodiorite) gneisses of peninsular India, occur as interlayering of granite, granite gneiss, and varying proportions of migmatitic gneiss [43].

2.2. Experimental Setup for Online Gas Monitoring at KFD1. The online mud gas monitoring was set up at the KFD1 drill site to determine and analyse the gases which are extracted from the drilling fluid. Gases were routinely monitored in one-minute intervals during all drilling phases (air hammer drilling, core drilling) and during water flushing from the borehole. However, only gas extraction and analysis during water flushing showed the presence of formation gases (i.e., nonatmospheric). Generally, gas from drilling mud comprises air and other components that are mechanically released either as the drill bit crushes the rock or when the drilling intersects permeable strata. The separation of gas from the drilling mud is done mechanically using a custom-built mud gas separator installed in the so-called "possum belly" at the head of the shale shaker screens. The mud gas is extracted from the returning mud and continuously pumped through a plastic tube to the on-site laboratory, where the gas composition is determined. Mud gas always contains a portion of air as the mud tanks and pumps are open to the atmosphere. The formation gases identified in drilling mud derive either from the pore space of the crushed rock or from fluids entering the borehole though open fractures/fault zones. The technique is operationally simple and comparatively inexpensive as it can be easily deployed on drill rigs and requires no additional rig time. However, the technique only works if drill mud circulation is established. The technical details for online mud gas monitoring are discussed in Erzinger et al. [7]. For air hammer drilling, pressurized air is applied in order to run the air hammer and to lift the cuttings to the surface. As the volume of atmospheric gases pumped down the hole is extremely high compared to the concentration of formation gases in crystalline rock, any formation gas that enters the borehole will be highly diluted. The cuttings are separated from the returning gas in a Mathena™ shale gas separator and a portion of the returning gas is introduced to the nearby OLGA laboratory through a plastic tube (Figure 2). The gas flow is adjusted with a flow meter and a membrane pump to build up vacuum, and a water trap condenses the water. On site, the dry gas is analysed with a quadrupole mass spectrometer (QMS, Pfeiffer OmniStar™ GSD 300 with mass range 0-100 amu) to determine relative gas concentrations. The gas is finally pumped through glass tubes for sampling gases for off-site isotope studies. With the present experimental setup at the KFD1 drill site, the gases N_2, O_2, Ar, CO_2, CH_4, He, and H_2 are determined at 1-minute sampling intervals with a detection limit of 1 ppmv (parts per million by volume). Prior to gas monitoring at Koyna, the mass spectrometer has been calibrated for the mass scale (to measure at the peak maximum) and for quantification of gas concentrations. For determination of gas concentrations, the measured ion currents are inputted to a solution matrix and the individual concentrations of the components in the gas to be analysed are determined via calibration factors. The calculated concentrations are automatically normalized to 100 vol.-%. Due to the normalization, the concentration determination is within a certain range independent of the inlet pressure of the gas. Nevertheless, the calibration measurements are performed at the same conditions, including gas inlet pressure, as for the gas monitoring experiment (atmospheric pressure).

The calibration factors used for concentration determination are calculated from the analysis of air and a certified gas mixture, composed of N_2 (64.2 vol.-%), CH_4 (30.3 vol.-%), CO_2 (5.12 vol.-%), ethane (1985 ppmv), propane (500 ppmv), Ar (499 ppmv), He (473 ppmv), and H_2S (454 ppmv). Since all calibration factors are given as relative values, a fixed calibration factor (internal standard) is defined with the value 1. In the present study, ^{40}Ar ($m/e = 40$) is used as the internal standard, where all other calibration factors relate to this value. Apart from determination of the calibration factors, the measurement of calibration gas is also used to determine the standard deviations of the measured values. For that purpose, ion currents are averaged over 11 measurement cycles, and the following relative 2σ standard deviation values are obtained for different gas concentration ranges: 100-0.1 vol.-%: ±1%, 1000-100 ppmv: ±2%, 100-10 ppmv: ±5%, <10 ppmv: ±10%.

During online measurements, a record of relative gas concentrations versus time is obtained. The data is later converted into gas concentrations versus depth using lag depth versus time data provided by a commercial mud logging company. The lag depth corresponds to the drill bit depth, corrected for the depth drilled during the time interval that the gas needs to reach the surface. During coring operations, the drilling mud is replaced by water after each coring run in order to prepare for air hammer drilling, as the lifting capacity of air hammer drilling is not sufficient to directly blow out the drilling mud of a mud-filled borehole. In the next step, the water in the borehole is progressively flushed out from top to bottom of the borehole in ~100 m intervals (Figure 3). Significant amounts of formation gases were detected when the water column was running through the Mathena™ separator. These observed gas enhancements represent the integrated concentration of gas in the respective ~100 m depth interval. Sixteen gas samples were collected from different depths in the granitic basement section during the water flushing after core runs, as listed in Table 1. With known total volume of the Mathena separator (~12 m^3) and water volume introduced to the separator (2.49-3.51 m^3), the absolute concentration of helium in each water column can be estimated. Table 1 shows the absolute helium

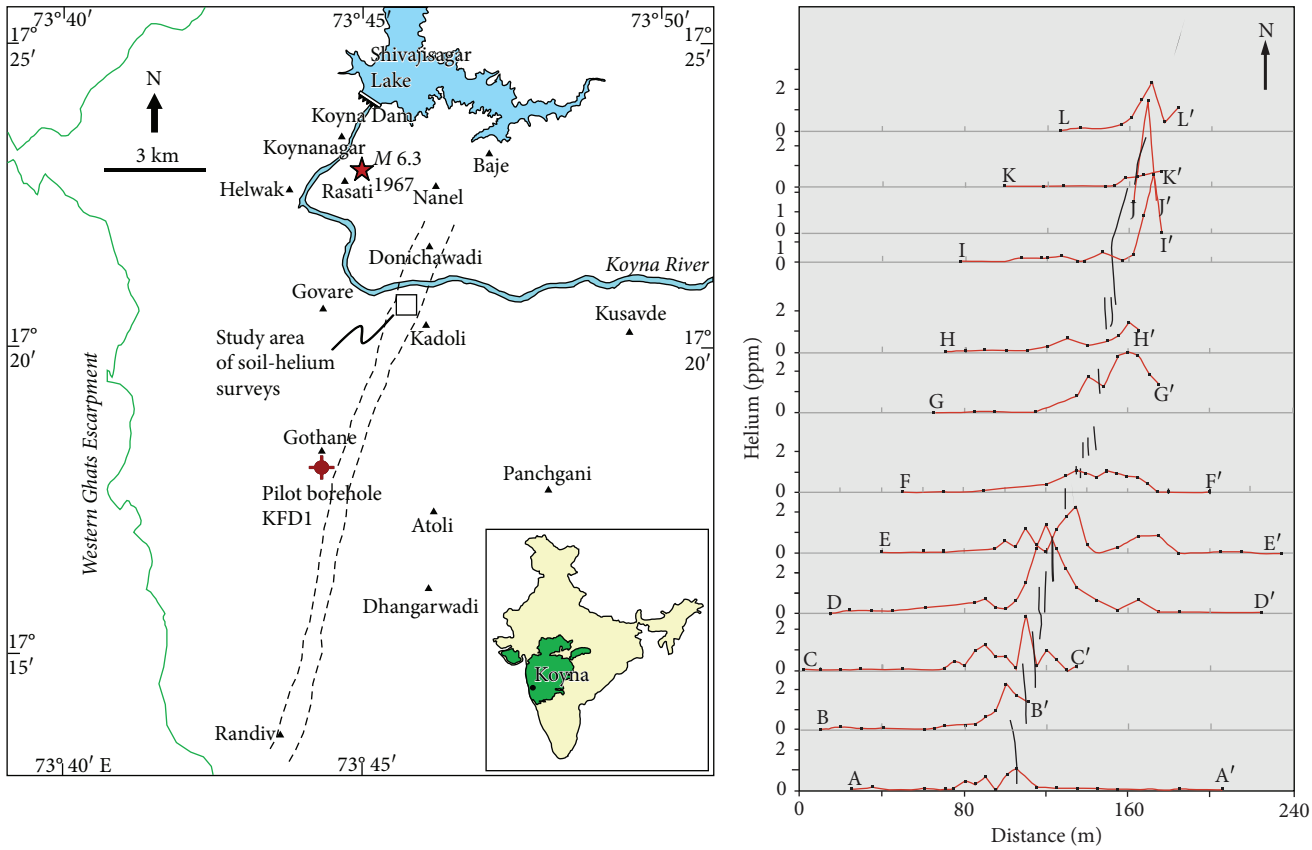

(a) (b)

FIGURE 1: (a) Map of the Koyna region showing the locations of the 1967 M 6.3 Koyna earthquake (red star) and the pilot borehole KFD1. The trace of the Donichawadi fissure zone (dashed lines), formed during 1967 earthquake [31, 40], and the study area (square) where the soil-helium surveys were conducted during 1996-1997 are also shown. Inset shows the location of Koyna within the Deccan Traps province (shaded green) on the outline map of India. (b) Map showing the coincidence of the helium anomalies established by soil-helium measurements along 12 traverses (AA′, BB′,..., LL′) with coseismic en echelon fissures (thick lines) from the 1967 earthquake (Gupta et al. [41]).

concentrations in each water column in millimole, corrected for atmospheric helium input, according to

$$\mathrm{He}_{\text{air-corrected}} = \mathrm{He}_{\text{measured}} - \left[\mathrm{He}_{\text{air}} * \frac{\mathrm{O}_{2(\text{measured})}}{\mathrm{O}_{2(\text{air})}}\right]. \quad (1)$$

Before the water column is introduced into the Mathena separator, the complete separator volume is exchanged several times with air. Hence, any input of residual gas from the degassing of the previous water column seems less likely, which is underlined by the observed significant variation in H_2 concentration between the sample RIH20 (139 ppmv) and the sample RIH21 (50 ppmv). Two core runs were separated by an interval of air hammer drilling, except the 5th and 6th core runs and the 7th and 8th core runs which were done consecutively.

2.3. Borehole Spectral Gamma Ray Logging. Spectral gamma ray logs were taken in association with geophysical well logging in the pilot borehole KFD1. A standard natural gamma ray spectrometry sonde from Schlumberger® was lowered in the borehole, and data was acquired in the open hole sections 500-1500 m and 1500-3000 m at a logging speed of 240 m/h. Prior to the measurements, the sonde was calibrated with reference sources of ^{40}K, ^{238}U, and ^{232}Th. The spectral gamma ray log measures the natural gamma radiation emanating from a formation split into contributions from each of the major radioisotopic sources K, Th, and U. The characteristic peaks in potassium at 1.46 MeV, the thorium series at 2.62 MeV, and the uranium series at 1.76 MeV are caused by the decay of ^{40}K and short-lived daughter products of the uranium (^{208}Tl) and thorium (^{214}Bi) decay chain. A multichannel analyser is used to determine the amount of radiation coming from the energies associated with each of these major peaks. From the response of the tool and the number of counts in each energy window, the individual concentrations of K, Th, and U in the formation are determined.

2.4. Laboratory Investigations. Sixteen gas samples are analysed with a QMS for the chemical gas composition (^{4}He, ^{40}Ar, N_2, O_2, CH_4, CO_2, and H_2), with a gas chromatographer (SRI 8610C) equipped with a flame ionization detector using hydrogen as the carrier gas for hydrocarbons

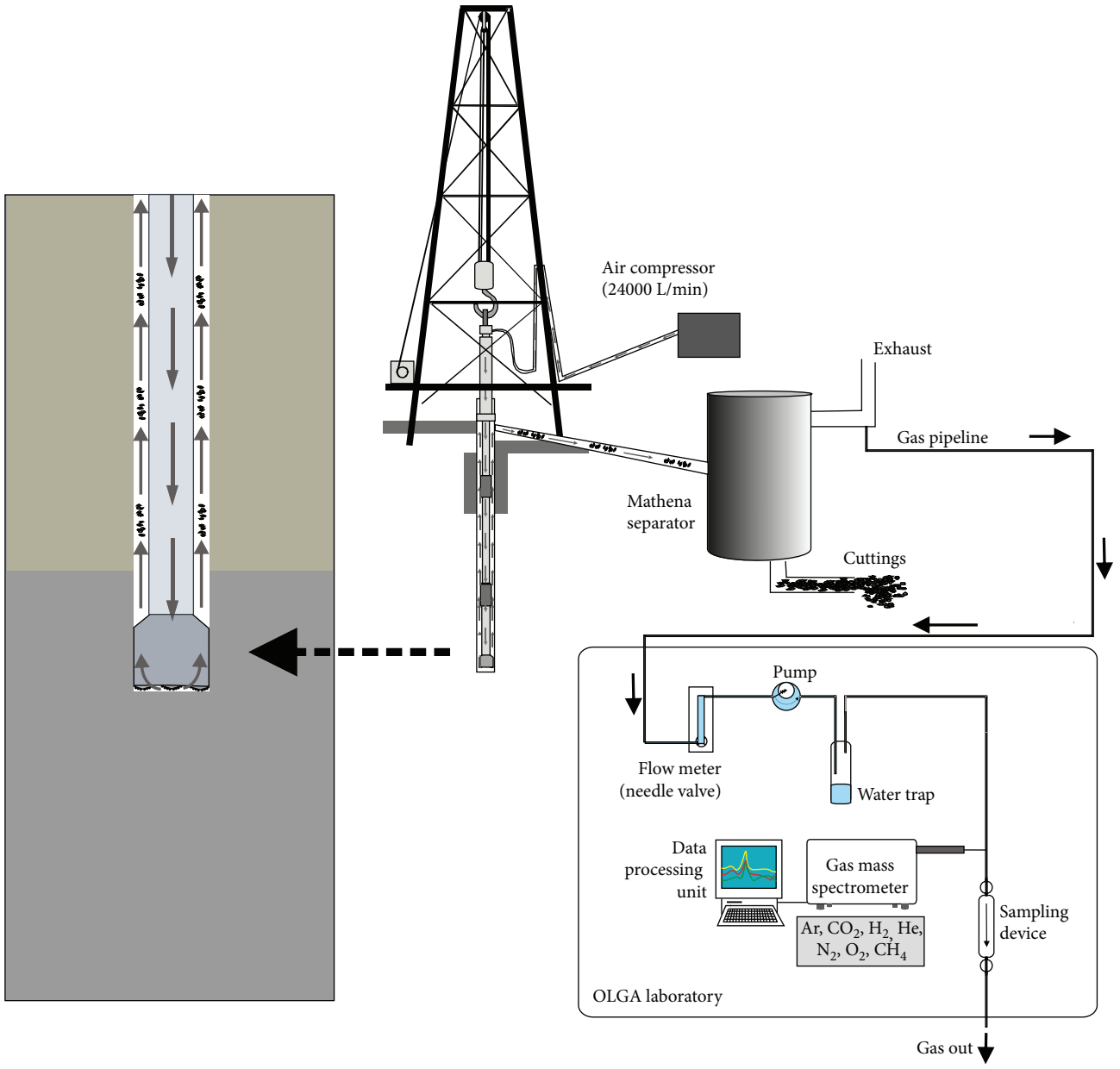

Figure 2: Schematic diagram showing the air hammer drilling setup and major components of the OLGA laboratory at the drill site. The Mathena shale gas separator is used to separate gas from borehole cuttings, and the gas is then pumped through a plastic tube to the nearby OLGA laboratory where the gases are determined.

(C1-C4). The gas chromatograph was calibrated with a reference gas (CH_4: 4990 ppmv, C_2H_6: 297.8 ppmv, C_3H_8: 200.3 ppmv, i-C_4H_{10}: 99.4 ppmv, n-C_4H_{10}: 101.7 ppmv, and residual gas: N_2 with traces of CO_2, H_2, and He), followed by eleven measurements of the calibration gas to determine accuracy and precision. Average values of the measurements deviate <2% from the calibration gas concentration for all measured gas species. Relative 2-sigma standard deviations are ≤1% for CH_4, ≤2% for C_2H_6 and C_3H_8, and ≤5% for i/n-C_4H_{10}, indicating that the determinations of all gas species were precise and unbiased.

Eleven samples are analysed for noble gas isotopes with a VG 5400 noble gas mass spectrometer. The following noble gas nuclides have been investigated with the noble gas mass spectrometer: ^{3}He, ^{4}He, ^{20}Ne, ^{21}Ne, ^{22}Ne, ^{36}Ar, ^{38}Ar, ^{40}Ar, ^{84}Kr, and ^{132}Xe. The procedure for noble gas isotope analyses includes gas purification, mass spectrometric analysis, and data processing and is briefly described in the following (see paper by Niedermann et al. [44] for details). A portion of gas with a predefined volume is introduced in the purification line at constant pressure. Water vapour is condensed in a dry-ice-cooled cold trap. Removal of nitrogen, oxygen, and carbon dioxide is accomplished by passing the sample to two titanium sponge getters, which are cyclically heated. Two Zr-Al getters extract hydrogen, hydrocarbons, and the remaining carbon dioxide. The cleaned gas is then transferred to two cryogenic cold heads. The former allows adsorption of argon, krypton, and xenon at 50 K

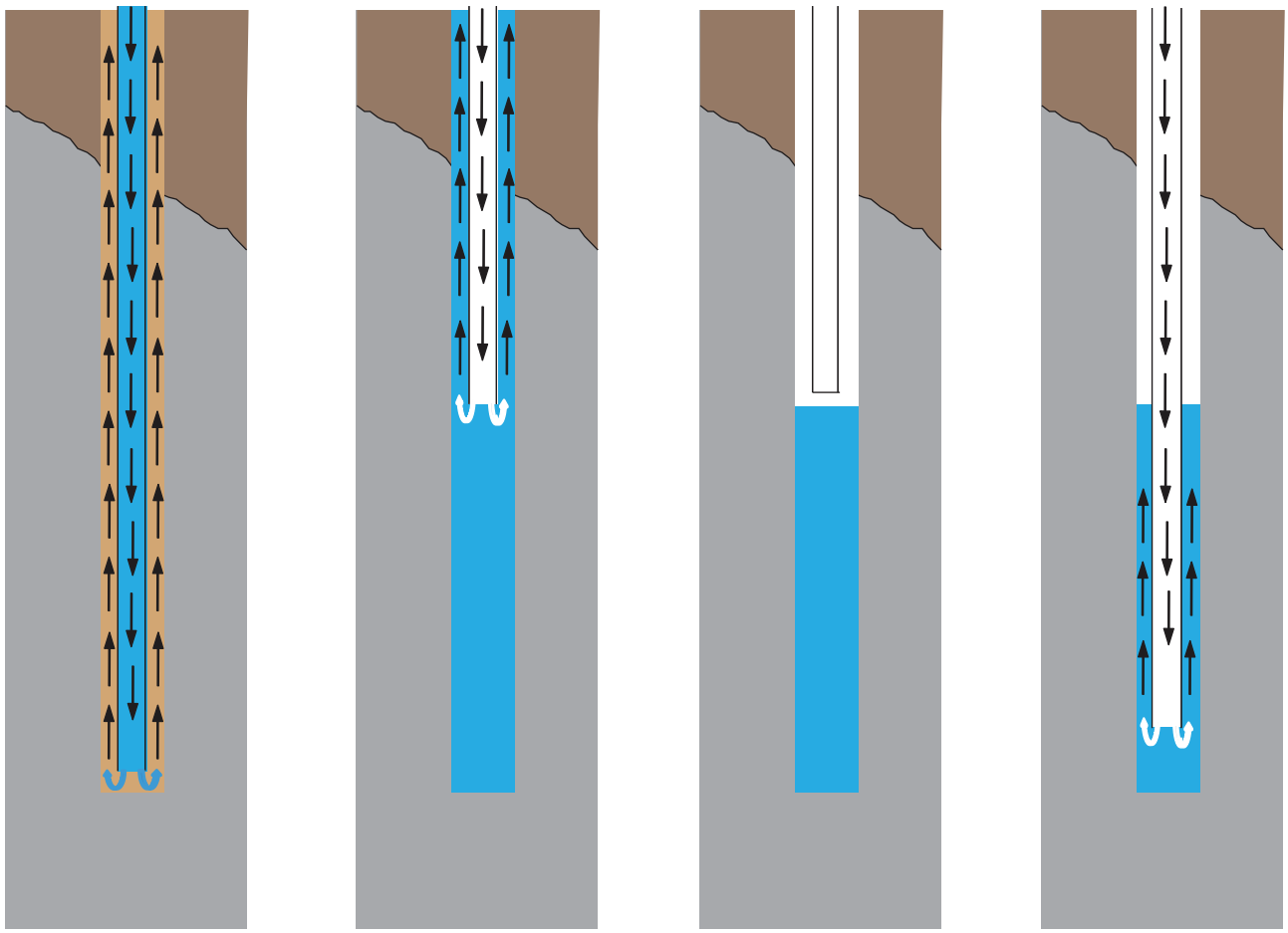

Figure 3: Schematic diagram showing (from left to right) replacement of drilling mud by water after each coring run, and the water in the borehole is then progressively flushed out from top to bottom of the pilot borehole KFD1 in ~100 m intervals.

temperature, while helium and neon are collected with the second cold head at 11 K. After noble gas adsorption at the cold heads, they are stepwise heated for individual noble gas release and determination. The second cryogenic cold head is heated to 35 K for helium and afterwards to 120 K for neon release. Background concentrations of argon and hydrocarbons are suppressed by a stainless steel frit and an activated charcoal finger that is cooled with liquid nitrogen. Ar, Kr, and Xe are released and measured together by heating the first cold head to 190 K. The measurements in this study are corrected for initial ("blank") gas concentrations and influences of atmospheric gas following Niedermann et al. [44]. Concentrations of the blanks are typically (in cm^3 STP) as follows: ^{4}He: ~5×10^{-12}, ^{20}Ne: ~0.5×10^{-12}, ^{40}Ar: ~5×10^{-10}, ^{84}Kr: ~0.05×10^{-12}, and ^{132}Xe: ~0.02×10^{-12} [44, 45]. These concentrations are well below the concentrations in the samples; therefore, a correction was not necessary. Systematic errors by, e.g., incorrect adjustment or inaccurate calibration may bias the accuracy of a noble gas measurement. Such systematic errors shift all measured values in a certain direction. These errors can only be estimated but are likely to be small compared to statistical errors in most cases. Determinable systematic errors in noble gas analytics are, for example, the time-dependent change of a measured value over the measurement time (up to 40 min) of the measurement cycles (typically 11). Such errors are corrected by extrapolation to the time of gas inlet into the mass spectrometer. All data have been corrected for isobaric interferences and mass discrimination effects. Error limits given in this paper correspond to 2-sigma standard deviations (95.5%) and include statistical uncertainties of the measurement as well as uncertainties of sensitivity and systematic errors of mass discrimination determinations, blanks, and interferences.

3. Data Processing and Results

Except for helium, all noble gas isotopic ratios of our study are indistinguishable from air. Due to clearly distinct helium isotope compositions of different reservoirs and the lower sensitivity for atmospheric contamination, helium isotopes constitute a capable tool to identify the origin of fluids from depth. Helium is not accumulated in the atmosphere, and therefore, the relative atmospheric concentration of helium is low (5.24 ppm). Helium isotope ratios are generally stated as ^{3}He/^{4}He and denoted in atmospheric ratios Ra ($[^3\text{He}/^4\text{He}]_{\text{air}} = 1.39 \times 10^{-6} = 1$ Ra). The continental crust is depleted in primordial noble gas nuclides, and its average

Table 1: Molecular composition of gas samples collected during water flushing after core run in the pilot hole KFD1 at Gothane, near Koyna, Western India.

Sample	Depth (m)	Flushing after core run #	^{40}Ar (vol.-%) (±1%)	CH_4 (ppmv) (±5%)	CO_2* (ppmv) (±2%)	H_2 (ppmv) (±5%)	He (ppmv) (±10%)	N_2 (vol.-%) (±1%)	O_2 (vol.-%) error = ±1%	C1 (ppmv)	C2 (ppmv)	C3 (ppmv)	i-C_4 (ppmv)	n-C_4 (ppmv)	He air-corrected (millimole)
RIH06	2084	5/6	0.983	10	965 (580)	57	6.1	77.8	21.1	14	—	0.4	—	0.3	n.d.
RIH07	2189	5/6	0.982	6	700 (310)	37	5.6	77.6	21.3	5	—	—	—	—	n.d.
RIH08	2295	5/6	0.985	14	32200 (31810)**	63	5.7	77.3	18.4	9	—	—	—	—	n.d.
RIH13	1737	7/8	0.985	48	1005 (620)	45	5.5	77.6	21.3	48	—	—	0.3	—	n.d.
RIH14	1833	7/8	0.996	46	940 (550)	41	6.2	77.7	21.2	60	—	—	—	0.4	0.34
RIH15	1929	7/8	0.999	62	655 (270)	44	7.2	77.6	21.3	65	—	—	0.3	—	0.71
RIH16	2025	7/8	0.991	70	985 (600)	62	7.5	77.8	21.1	69	—	0.3	0.3	—	0.84
RIH17	2121	7/8	0.995	66	930 (540)	34	7.6	77.5	21.4	62	—	—	—	—	0.85
RIH18	2217	7/8	0.992	186	1200 (810)	78	12.8	77.8	21.0	180	—	0.4	—	0.4	2.86
RIH19	2313	7/8	0.989	88	1160 (770)	49	10.1	77.7	21.1	96	—	1.2	—	—	1.83
RIH20	2409	7/8	0.999	140	1180 (790)	139	11.1	77.8	21.1	104	—	—	0.3	—	2.21
RIH21	2514	7/8	0.980	76	1050 (660)	50	10.6	77.8	21.0	66	—	—	—	—	1.95
RIH22	2610	7/8	0.995	52	820 (430)	44	9.9	77.7	21.2	48	—	0.3	0.3	0.6	1.74
RIH23	2687	7/8	0.989	86	970 (580)	46	12.7	77.9	21.0	n.d.	n.d.	n.d.	n.d.	n.d.	3.05
RIH24	2763	7/8	0.999	88	1065 (680)	52	10	77.9	20.9	103	—	—	—	—	1.96
RIH25	2831	7/8	0.992	96	875 (490)	55	9.8	77.9	21.0	78	—	0.5	0.5	0.8	1.93

Gas samples collected during running in and flushing out of water are designated by the prefix RIH. Depths are referenced to the kelly bushing, which was located at 3.5 m elevation with respect to ground level. *Values in parentheses are air-corrected according to $[CO_2]_{air-corrected} = [CO_2]_{measured} - ([O_2]_{measured} \times [CO_2]_{air}/[O_2]_{air})$. **Probably an artefact from sample preparation. —: below detection limit (=0.3 ppmv); n.d.: not determined.

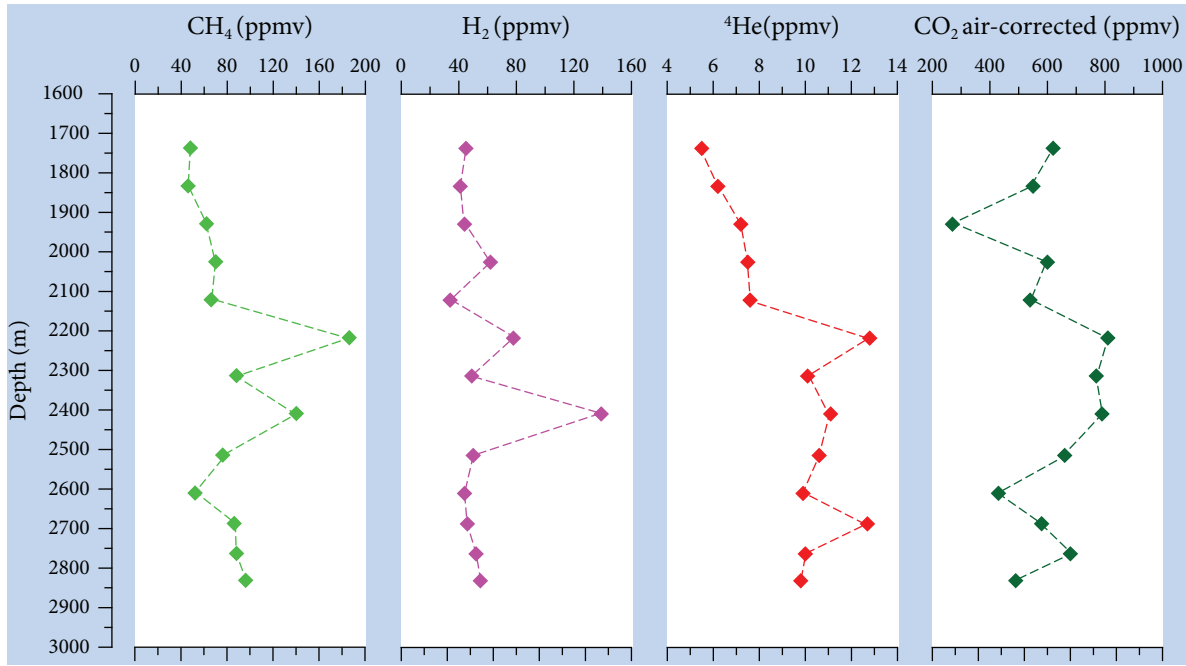

Figure 4: Plot showing concentration versus depth profiles of CH_4, H_2, ^4He, and CO_2 obtained from measurements on gas samples collected during water flushing after core run 7/8.

helium isotope composition (<0.05 Ra) is governed by ^3He from the reaction ^6Li (n,α) $^3H(\beta^-)$ ^3He and ^4He from the decay of uranium and thorium. Sublithospheric, asthenospheric, and deep mantle reservoirs are characterized by $^3He/^4He$ ratios of >1 Ra.

Correction of the measured helium isotopic ratios for atmospheric helium is required as gas samples contain a contribution of atmospheric gases. $^4He/^{20}Ne$ or $^4He/^{36}Ar$ ratios are mostly used to determine the degree of atmospheric contamination. ^{20}Ne and ^{36}Ar are both primordial, i.e., only to a negligible extent affected by ingrowth through radiogenic, nucleogenic, or fissiogenic processes in the continental crust. For our study, the $^4He/^{20}Ne$ ratio is used to correct the measured $^3He/^4He$ ratios in the gas samples according to a method first described by Craig et al. [46], assuming that the continental crust is depleted in primordial noble gas nuclides and ^{20}Ne completely derives from the atmosphere.

Online gas monitoring during drilling has been performed in the Koyna pilot borehole KFD1 starting from the 1315 m to 2831 m depth in the granite-gneiss basement section. In the case of air hammer drilling, the formation gases suffered dilution with the air that was pumped into the borehole, as evident from the gas concentrations that are similar to that of air. Similarly, for the rare cases of mud drilling, no formation gases are detected as the volume of the drilled rock was very low compared to the drilling mud that was pumped downhole. We therefore do not report any gas data from air hammer drilling and mud drilling. The present study is based on data mostly from gas monitoring during water flushing and off-site laboratory studies on gas samples.

The formation gases analysed from online gas monitoring in the 1642-2831 m section during water flushing after the 7th and 8th coring runs are plotted in Figure 4. Sixteen gas samples from 1737 m to 2831 m are analysed for N_2, O_2, Ar, CO_2, CH_4, H_2, and He. The molecular composition of the gas samples is reported in Table 1. Online gas monitoring together with laboratory analyses of gas samples show that the most abundant formation-derived gases from KFD1 are CO_2, CH_4, H_2, and He. The other gases such as N_2, O_2, and Ar derive from the atmospheric input in the drilling fluid, as indicated by relative proportions of concentrations of these gases indistinguishable from air. All hydrocarbons (C_2H_6, C_3H_8, i-C_4H_{10}, and n-C_4H_{10}) except CH_4 show negligible concentrations. Therefore, the present work emphasises on CO_2, CH_4, H_2, and He data sets. The concentrations of CO_2 reach up to 1200 ppmv (excluding an outlier with 32200 ppmv), CH_4 up to 186 ppmv, H_2 up to 139 ppmv, and He up to 12.8 ppmv. The data also indicates that most gas-rich zones generally occur below the 2100 m depth in the borehole. The measured helium concentrations are observed to be low at ~1800 m, increase substantially at the ~2217 m depth, and maintain the increased level up to the ~2831 m depth. Two prominent peaks, between 2121 m and 2217 m and between 2610 m and 2687 m, are observed.

Eleven gas samples collected from the depth section 1833-2831 m are also analysed for noble gas isotopes. Except for helium, abundances and isotope ratios of all noble gases are atmospheric and not reported here. The measured values of $^4He/^{20}Ne$ and $^3He/^4He$ along with air-corrected $^3He/^4He$ ratios, the atmospheric contribution to the total helium, and the crustal and mantle-derived helium are listed in Table 2. Air correction of helium isotope ratios has been applied as $^4He/^{20}Ne$ ratios for all the samples in the present study are higher than the atmospheric component of 0.319. The data shows that the measured $^3He/^4He$ ratios are in the range 0.43-0.91 Ra, with $^4He/^{20}Ne$ values between 0.34 and

Table 2: Noble gas composition of gas samples collected during water flushing after core run 7/8 in the pilot hole KFD1 at Gothane, near Koyna, Western India.

Sample	Depth (m)	^{4}He (ppmv)	±	^{20}Ne (ppmv)	±	^{40}Ar (ppmv)	±	^{4}He/^{20}Ne	±	^{3}He/^{4}He (Ra)	±	Crustal contribution (%)	Atmospheric contribution (%)
RIH14	1833	5.96	0.67	17.5	2.0	9900	1100	0.3449	0.0091	0.912	0.059	7.5	92.5
RIH15	1929	6.67	0.75	16.6	1.9	9400	1100	0.406	0.011	0.782	0.032	21.4	78.6
RIH16	2025	7.88	0.88	17.5	2.0	10000	1100	0.455	0.012	0.705	0.036	29.8	70.2
RIH17	2121	7.12	0.80	16.4	1.8	9300	1000	0.440	0.012	0.703	0.050	27.5	72.5
RIH18	2217	12.8	1.4	17.1	1.9	9300	1000	0.751	0.020	0.426	0.022	57.5	42.5
RIH19	2313	10.7	1.2	17.3	1.9	9700	1100	0.624	0.017	0.522	0.027	48.9	51.1
RIH20	2409	12.2	1.4	18.2	2.0	10200	1100	0.682	0.018	0.482	0.034	53.2	46.8
RIH21	2514	11.3	1.3	17.3	1.9	9900	1100	0.659	0.017	0.479	0.020	51.6	48.4
RIH22	2610	10.2	1.1	17.3	1.9	9900	1100	0.593	0.016	0.547	0.028	46.2	53.8
RIH24	2763	9.8	1.1	17.1	1.9	9800	1100	0.574	0.015	0.546	0.018	44.4	55.6
RIH25	2831	10.2	1.1	17.6	2.0	9900	1100	0.588	0.016	0.556	0.030	45.7	54.3

Depths are referenced to the kelly bushing, which was located at 3.5 m elevation with respect to ground level. Gas samples collected during running in and flushing out of water are designated by the prefix RIH. All errors are 2σ.

0.71, which confirms that the samples are a mixture of atmospheric helium and helium from crustal heat production. The low isotope ratios (<1) further confirm that there is no mantle contribution within the analytical uncertainties. The measured ^{4}He/^{20}Ne ratios are higher for gas samples below the 2100 m depth (Figure 5(a)). Assuming a value of 0.319 for the ^{4}He/^{20}Ne ratio for the atmospheric component, the calculated contribution of air in our samples ranges from 43% to 93% with an average value of 61%. Within 2σ analytical uncertainties, the mantle contribution to the total helium budget is zero for all samples. All samples are a mixture of atmospheric helium and helium from crustal origin (i.e., helium from radioactive decay of uranium and thorium in the continental crust). The same can be seen in the diagram ^{3}He/^{4}He versus ^{4}He/^{20}Ne (Figure 5(b)), where all data fall on a hyperbolic mixing curve between air and a crustal helium end-member with ^{3}He/^{4}He = 0.02 (i.e., the average crustal production ratio, [47, 48]).

3.1. Comparison between Helium Concentrations from QMS and Noble Gas Isotope Measurements. A comparison has been made between ^{4}He concentrations obtained from QMS and noble gas isotope measurements for the depth section 1737-2831 m. The mass resolution of the QMS is not sufficient to separate ^{3}He ($m = 3.016$) from HD ($m = 3.022$); therefore, ^{3}He can only be determined by noble gas isotope mass spectrometer measurements. Two samples from the 1737 m and 2687 m depth were not analysed for noble gas isotopes, and therefore, ^{4}He concentration from isotope analysis for those samples are not reported here. As shown in Figure 6, ^{4}He concentrations from QMS (Table 1) and from noble gas isotope mass spectrometer measurements (Table 2) are in good agreement. Noble gas concentrations determined by noble gas isotope mass spectrometer measurements have been calculated from noble gas nuclide pressure and gas sample inlet pressure. The latter was determined during QMS analysis. We assume that the sample pressure measured by the QMS corresponds to the gas sample inlet pressure when being introduced to the gas line of the noble gas isotope mass spectrometer measurements. The volume of our sample cylinders for all samples is 250 cc. Given a dead volume of 2 cc for the gas inlet, pressure reduction at the sample inlet in the gas line of the noble gas isotope mass spectrometer is <1%.

In contrast to helium concentrations measured by the noble gas isotope mass spectrometer, the helium concentrations measured by QMS are automatically normalized to 100% as total gas concentration. If the QMS measurement considers all gas species present in the gas phase, then both methods should result in the same helium concentration values (in ppmv). A comparison between the two data sets shows a discrepancy in helium concentration values in the range 0.4-9.9% with an average value of 4.9% and no systematic trend. For four samples, the QMS measurement yields higher helium concentration values, whereas seven samples show the opposite. Given an analytical uncertainty of ~10% for helium concentrations, determined by both methods, the agreement between both data sets is convincing.

4. Discussion

The maximum helium concentrations detected in the 3 km deep pilot borehole KFD1 at Gothane is 12.8 ppmv (by both QMS and noble gas isotope measurements), more than 7 ppmv higher than the atmospheric helium abundance of 5.24 ppmv. Earlier soil-gas helium surveys followed by core drilling carried out between 1995 and 1997 across the Donichawadi fissure zone near Kadoli village provide strong evidence that the fissure zone represents the surface rupture zone of the 1967 earthquake [41]. Helium concentrations exceeding the atmospheric value by 1-7 ppmv coinciding with the surface fissures, which fall off sharply to background value of 0.2 ppmv above atmosphere at a distance of 40-60 m on either side of the fissures, confirm that the fissures constitute the surface expression of a NNE-SSW-oriented seismic fault and that the fault zone had not healed even 30 years after the 1967 earthquake (Figure 1(b)). Elevated helium concentrations detected at depths below 2100 m in the Koyna

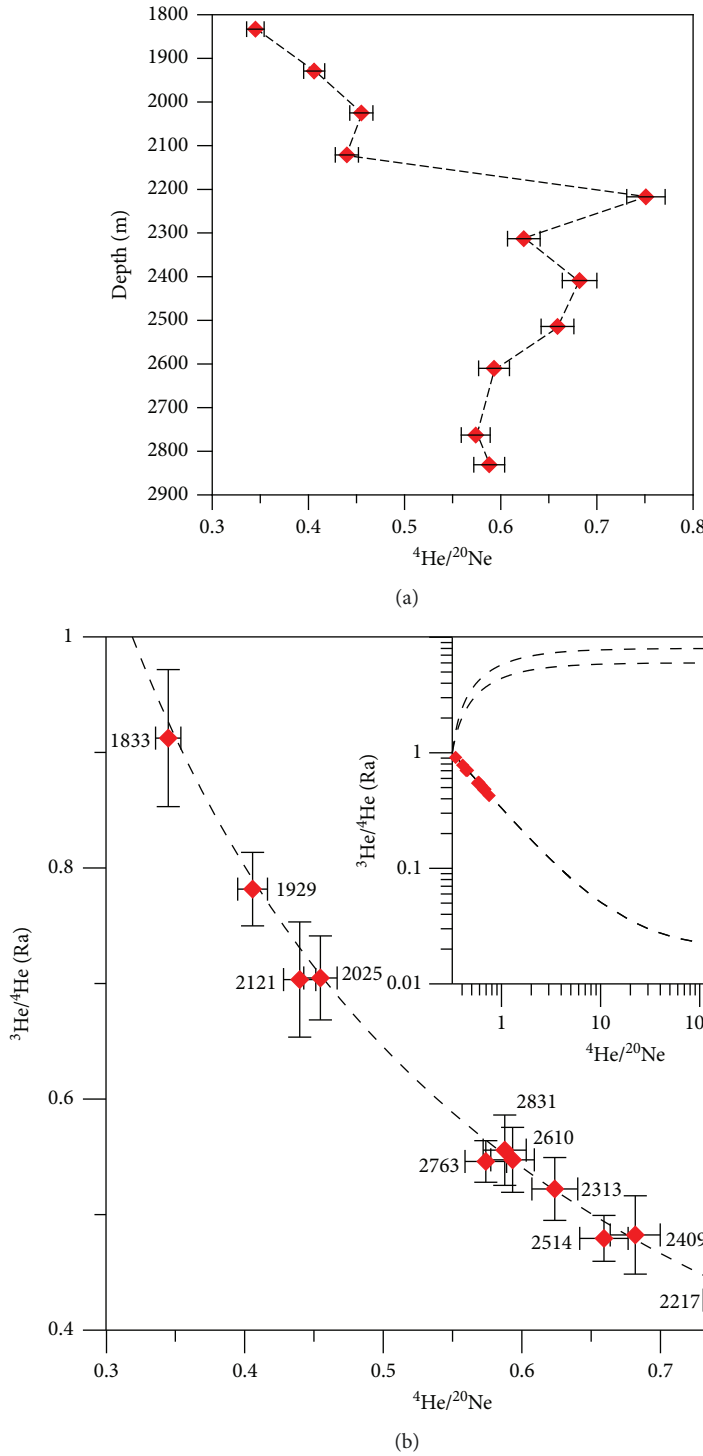

FIGURE 5: Plot showing (a) $^4He/^{20}Ne$ versus depth and (b) $^4He/^{20}Ne$ versus $^3He/^4He$, obtained from isotope measurements on gas samples collected during water flushing after core run 7/8. Error bars indicating uncertainty in the measurement are also shown. Depth of samples in "m" is indicated along with data points in (b). Inset shows mixing hyperbola between air and the continental crust and two different mantle end members (6 Ra for the lithospheric and 8 Ra for the asthenospheric mantle).

pilot borehole KFD1 of the present study are comparable to concentrations observed more than 20 years ago in the Donichawadi fissure zone. Additionally, $^3He/^4He$ and $^4He/^{20}Ne$ data from the present study reveal that helium gas obtained from the pilot borehole comprises atmospheric helium and variable contributions of crustal radiogenic helium with no mantle helium.

In general, helium could be a mixture of atmospheric helium ($^3He/^4He = 1$ Ra; [46, 47]) with different contributions of crustal helium ($^3He/^4He < 0.1$ Ra) and mantle-

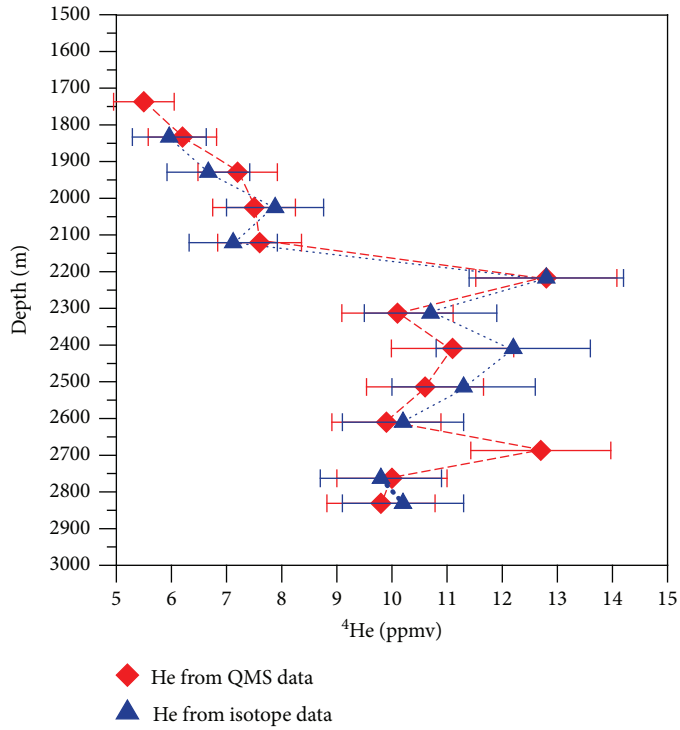

Figure 6: ^{4}He depth profiles from QMS measurements (red) and noble gas isotope analysis (blue) of gas samples collected during water flushing after core run 7/8. Error bars indicating uncertainty in the measurement are also shown. Samples from 1737 m and 2687 m depths were not analysed for noble gas isotopes.

derived helium (^{3}He/^{4}He > 1 Ra, e.g., 6 Ra for the lithospheric mantle; [49]). Measured ^{3}He/^{4}He ratios from three soil-gas samples collected above the Donichawadi fissure zone fall between 0.59 and 0.63 Ra [41]. The reported ^{3}He/^{4}He ratios are not air-corrected, leaving open the question of any possible mantle contribution to the total helium budget. With measured helium concentrations of up to 12.24 ppmv (7 ppmv excess helium plus 5.24 ppmv atmospheric helium) and helium isotope compositions of 0.59-0.63 Ra in soil-gas samples, a mantle-derived helium contribution of ~2% would be possible assuming ^{20}Ne concentrations of 16.48 ppmv (atmospheric value). If indeed the Koyna fault gas would contain such a small but significant contribution of a mantle-derived component, questions would arise on the provenance of mantle helium at Koyna (e.g., mantle plume degassing) and its migration mechanisms. Basu et al. [50] determined helium isotope ratios of rock samples from two Deccan alkaline complexes from northern India to be 10–13 Ra. The authors interpret their findings as evidence to support a lower mantle plume origin of Deccan Traps volcanism. Our data, however, clearly point out that no mantle-derived helium is present in any of the samples obtained from the borehole KFD1.

The present study shows that formation gases (CO_2, CH_4, H_2, and He) mostly enter the borehole below 2100 m, with a number of zones of significant He enhancement ranging from 4.6 to 7.6 ppmv above the atmospheric value. The observed gas-rich zones at depths below 2100 m have been compared with data from downhole geophysical logging acquired in the borehole KFD1 [51]. The gas-rich zones correlate well with the zones of anomalous physical and mechanical properties identified from geophysical logs. For comparison, the resistivity and caliper logs are plotted along with the helium concentrations (Figure 7). The logs show a number of localized zones of low resistivity below 2000 m that correspond with the zones of helium enhancement. A number of such zones are also associated with substantial enlargement in borehole diameter. The enlargement in borehole diameter in the form of cavities or washout zones is likely due to the presence of fracture zones in the formation. Electrical (FMI®) and acoustic (UBI®) images acquired in the borehole have shown that these zones contain high fracture density with large number of open fractures, majority of which are oblique to subvertical in orientation. Two typical zones with high fracture density, 2141-2151 m and 2619-2629 m, discovered by electrical and acoustic borehole image logs are shown in Figure 7. These zones are in good agreement with those of gas enrichment observed in our study. On the whole, the present study indicates that the borehole has punctured multiple fracture zones in the subsurface. The association of low resistivity zones with high helium concentrations indicates that the open fractures act as potential pathways for fluid flow in the borehole.

The borehole KFD1 is located ~5 km to the south of Kadoli along the trend of the Donichawadi fault zone (Figure 1(a)). The consistency in concentrations and isotope ratios of soil-gas helium over the fissures near Kadoli and helium from different depths below 2100 m in the borehole KFD1 suggests that the pilot borehole intersects the southward extension of the Donichawadi fault zone

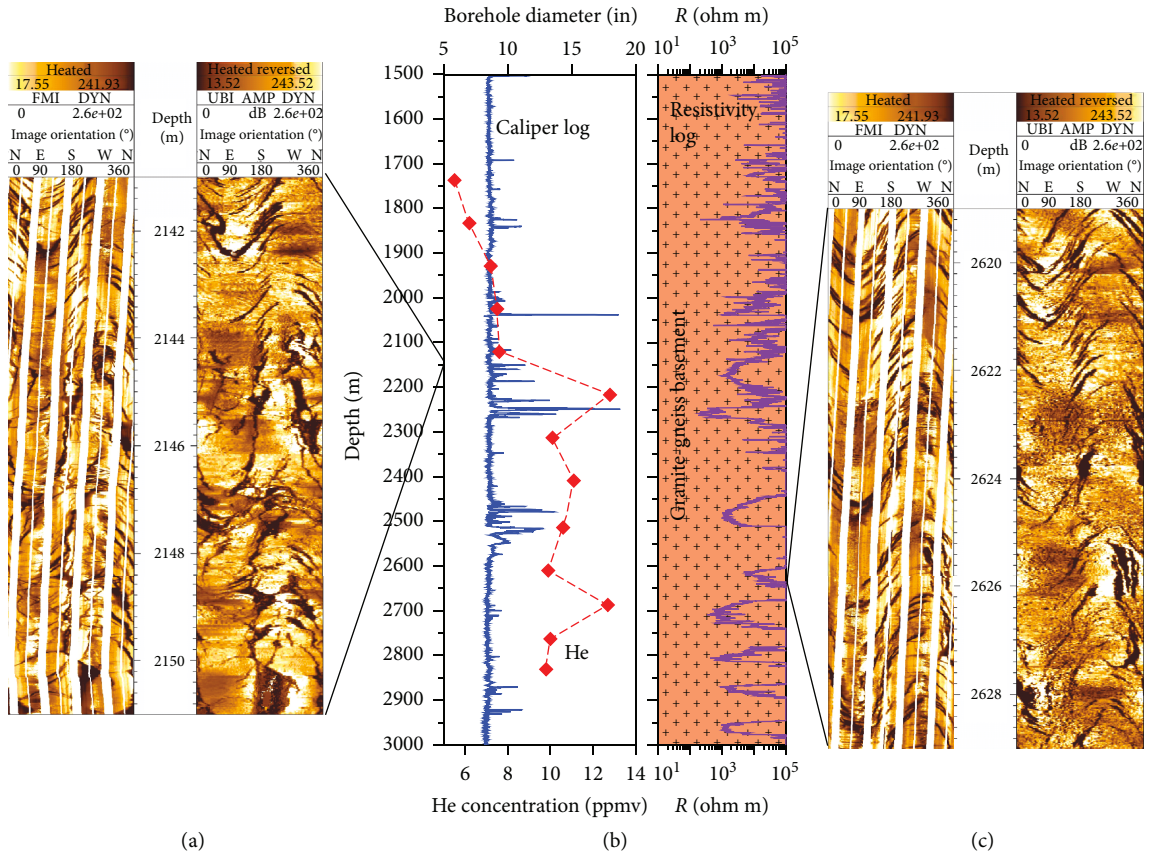

FIGURE 7: Plots showing downhole electrical resistivity (purple line) and calliper (blue line) logs along with helium concentration from QMS measurements (red diamonds) in the granitic basement section 1500-3000 m in the borehole KFD1. High resolution electrical (FMI) and acoustic (UBI) images of two typical depth sections 2141-2151 m (a) and 2619-2629 m (c) showing highly fractured basement rocks corresponding to zones of helium enhancements are also shown.

or its subsidiaries at multiple depths below ~2100 m. Results obtained from both the soil-helium gas study in the Donichawadi fault zone near Kadoli and the present study in the pilot borehole KFD1 demonstrate the possible connection of the Donichawadi fault through fractures zones where the gases migrated from the formation through media such as a borehole. Misra et al. [52] combined field investigations as well as physical and microstructural studies on basement core samples obtained from a 1522 m deep borehole at Rasati near Koyna to demonstrate the extension of the surface fissures into the granite-gneiss basement rocks at different depths beneath the Deccan flood basalt pile. They also suggested the association of these fissures with localized fault zones within the rock unit. Seismological studies including the analysis of seismograms recorded at a local network of 23 surface broadband stations and 6 borehole seismic stations show a distinct NNE-SSW trend of seismicity coinciding with the Donichawadi fault zone, indicating that the fault is still active [53, 54]. This inference gains support from other studies carried out in the Koyna region. Shashidhar et al. [55] carried out detailed studies on the M_w 4.8 earthquake of 14 April 2012, which is among the best monitored and well characterized events in the Koyna region. Using the amplitude inversion and the moment tensor inversion techniques, they show that the depth distribution of the aftershocks defines a NNE-SSW-trending fault plane dipping about 78° to the WNW, which is consistent with the trend of the Donichawadi fault. Shashidhar et al. [56] studied the earthquakes that occurred during January 2016 and May 2017 in the Koyna region and found that the seismicity is mostly confined to the Donichawadi fault zone during the reservoir drawdown phase (January-May) but occurred in a wider region during the reservoir-refilling phase (June-December). They attributed this pattern to the effect of pore pressure growth and retreat of the pressure front during loading and unloading cycles of the reservoir, respectively. All these studies point out that the seismicity in the Koyna region is mostly concentrated in the vicinity of the Donichawadi fault, which is still controlling the seismotectonics of the Koyna region even 50 years after the occurrence of the 1967 Koyna earthquake.

The present study shows that helium concentration is relatively low above the ~2121 m depth (≤7.6 ppmv) followed by a sudden increase of helium at ~2217 m (12.8 ppmv) which is maintained (9.8-12.7 ppmv) up to ~2831 m. To understand the variations with depth, helium data has been compared with Th and U data obtained from the spectral gamma ray log in the borehole KFD1. The decay chains of ^{235}U, ^{238}U, and ^{232}Th are the main sources of radiogenic helium. The proportion of uranium and thorium for the

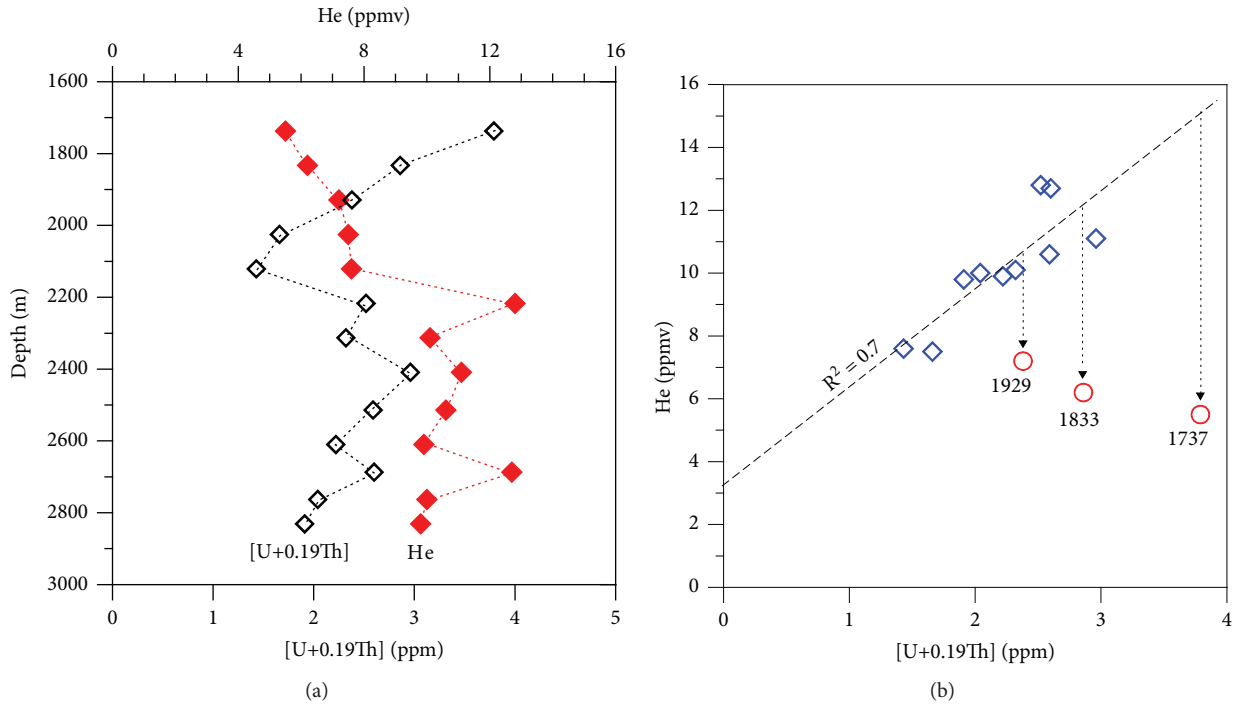

FIGURE 8: (a) Plot showing depth distribution of [U+0.19Th] (black open diamonds) and He (red diamonds). [U+0.19Th] values are averaged over the same ~100 m depth intervals as the depth of the water columns from where helium was extracted. (b) Correlation diagram for He versus [U+0.19Th]. Blue open diamonds indicate data from below 2100 m depth, where a positive correlation ($R^2 = 0.70$) is obvious. Red open circles are data from shallower depth which might be affected by helium loss (degassing).

current production of ^{4}He is [U+0.24Th], sometimes called "effective uranium" (eU). Due to different half-life times of uranium and thorium, this proportion is not constant over geological times and is time-integrated for the last 2.7 Ga (age of the crystalline basement rocks [57]), [U+0.19Th].

Plotting helium concentrations against [U+0.19Th], averaged over the same ~100 m depth intervals as for helium, displays a positive correlation for all data points below 2000 m (Figure 8). A linear fit ($R^2 = 0.70$) yields 3.14 ppmv helium per ppm [U+0.19Th]. An interesting observation is that for the shallow samples (<2000 m), the correlation between [U+0.19Th] and He is not valid. Assuming that the downhole logging data for U and Th are appropriate, the corresponding helium concentration should be between 10 and 14 ppmv, much higher than observed (≤7 ppmv, Figure 8). The helium-bearing water column from depths < 2000 m may therefore have undergone significant loss of helium. A possible explanation for helium lost from the water column would be partial helium degassing in the upper two kilometres of the water column in the borehole [48, 58]. Other mechanisms to explain the apparent helium lost in the upper part of the borehole, e.g., diffusion or lower permeability, are less suitable to explain the trend of increasing helium lost with shallower depth.

It should be noted that for all gases investigated in our study (CH_4, CO_2, H_2, and He), significant increase of gas concentrations is observed below the 2100 m depth (Figure 4). Helium (radiogenic) and hydrogen (radiolytic) might be produced by U and Th decay in situ, but this is a little likely for CO_2 and CH_4. Organic material, which could serve as a source for in situ production of CO_2 and CH_4, was not reported in cuttings and cores from KFD1. Moreover, the possibility for generation of organic matter in intact granite-gneiss formation is extremely remote. The only possibility appears to be fracture zones intersecting the borehole in the granitic basement that could serve as potential locales of organic matter or siderophilic bacteria transported along with fluids from the overlying rock mass. As described in the previous section, the granitic basement formation below the 2000 m depth is highly fractured at several depths, which may provide the favourable pathways for fluids to flow in the borehole. Moreover, it is also not clear whether U and Th are located in the rock matrix, as fluids in the fractures could have served as carriers for U and Th. We therefore interpret the helium data as partially deriving from formation pore space around the borehole and partially flowing through open fractures in the borehole. This indicates fluid-controlled migration through permeable strata such as fractures/faults at depths below 2100 m resulting in high helium concentrations relative to depths above 2100 m. Eventually, the presence of permeable fracture/fault zones will have important implications for the pore pressure evolution at depths and the occurrence of reservoir-triggered earthquakes in the Koyna region.

In the present study, online gas monitoring has not shown significant inflow of formation gases during both air hammer and mud drilling. In the case of the former, formation gases in crystalline rock were diluted with the volumes of air pumped down the hole, and in the case of the latter, this was due to the mud weight and the lower

surface to volume ratio of the drill core. However, as gas extraction and analysis during water flushing following each core run showed the presence of anomalous formation gases, the study opens up a new approach to study crustal gases in such scenarios.

Our study, together with the results from the previous soil-gas helium study, demonstrates the presence of helium at seismogenic depths in this region. This suggests that continuous monitoring of deeper gas emanations in the subsurface could be useful to understand temporal gas variations in the fault zones, which in turn could be useful for earthquake precursory studies in this region.

5. Conclusions

Online gas analyses and off-line noble gas isotope studies on eleven gas samples collected during water flushing in the Koyna pilot borehole KFD1 brings out the following conclusions:

(1) Formation gases (CO_2, CH_4, H_2, and He) mostly enter the borehole at different depths below 2100 m, with significant He enhancement ranging from 4.6 to 7.6 ppmv above the atmospheric value. The He-rich zones correlate well with the zones of anomalous physical and mechanical properties delineated from geophysical logs and are characterized by high fracture density as revealed from borehole images, indicating fluid-controlled migration through permeable strata such as fractures/faults at those depths

(2) The helium concentrations measured in the borehole below the 2100 m depth are in good agreement with the concentrations observed at the surface more than 20 years ago, which confirms that the Donichawadi fault zone is still permeable, 50 years after the 1967 *M* 6.3 Koyna earthquake

(3) Air-corrected helium isotope ratios indicate that helium is composed of atmospheric helium and variable contributions of crustal radiogenic helium with no mantle helium input within 2σ analytical uncertainties

(4) The presence of helium at seismogenic depths in this region is evident; however, a deeper understanding of fluid migration in time and space and its link to fault processes requires further investigations

Data Availability

The datasets used to support the findings of the study are included within the article.

Conflicts of Interest

The authors declare that they have no conflicts of interest.

Acknowledgments

We thank the Secretary to the Government of India, Ministry of Earth Sciences, for the support and encouragement in carrying out scientific drilling and associated studies in the Koyna region. This work was carried out in collaboration with the International Continental Scientific Drilling Program (ICDP). We are grateful to Harsh Gupta for steering the programme on scientific deep drilling at Koyna and for extended field discussions during the course of the study. Shailesh Nayak provided critical geological inputs during planning and execution. Vyasulu V. Akkiraju, Digant Vyas, Ashish Warhade, and Dinesh Nikalje provided invaluable help during gas monitoring at the drill site, and Deepjyoti Goswami helped with interpretation of image logs. Shivganga Drillers provided valuable logistic support at the drill site. Noble gas isotope analysis was performed at the GFZ Potsdam noble gas laboratory (Section 3.1); we are grateful to Samuel Niedermann and Enzio Schnabel for the tremendous help. The manuscript has benefited from constructive suggestions from two anonymous reviewers. We thank the Director, NCPOR, for facilitating the studies.

References

[1] S. Hickman, R. Sibson, and R. Bruhn, "Introduction to special section: mechanical involvement of fluids in faulting," *Journal of Geophysical Research: Solid Earth*, vol. 100, no. B7, pp. 12831–12840, 1995.

[2] J. R. Rice, "Fault stress states, pore pressure distributions, and the weakness of the San Andreas Fault," *International Geophysics*, vol. 51, pp. 475–503, 1992.

[3] A. Gudmundsson, "Fluid overpressure and stress drop in fault zones," *Geophysical Research Letters*, vol. 26, no. 1, pp. 115–118, 1999.

[4] J. Imber, R. E. Holdsworth, S. A. F. Smith, S. P. Jefferies, and C. Collettini, "Frictional-viscous flow, seismicity and the geology of weak faults: a review and future directions," *Geological Society, London, Special Publications*, vol. 299, no. 1, pp. 151–173, 2008.

[5] P. Möller, S. M. Weise, E. Althaus et al., "Paleofluids and recent fluids in the upper continental crust: results from the German Continental Deep Drilling Program (KTB)," *Journal of Geophysical Research: Solid Earth*, vol. 102, no. B8, pp. 18233–18254, 1997.

[6] W. Bach, D. Naumann, and J. Erzinger, "A helium, argon, and nitrogen record of the upper continental crust (KTB drill holes, Oberpfalz, Germany): implications for crustal degassing," *Chemical Geology*, vol. 160, no. 1-2, pp. 81–101, 1999.

[7] J. Erzinger, T. Wiersberg, and M. Zimmer, "Real-time mud gas logging and sampling during drilling," *Geofluids*, vol. 6, no. 3, 233 pages, 2006.

[8] G. V. Rao, G. K. Reddy, R. U. M. Rao, and K. Gopalan, "Extraordinary helium anomaly over surface rupture of September 1993 Killari earthquake, India," *Current Science*, vol. 66, no. 12, pp. 933–935, 1994.

[9] G. K. Reddy, G. V. Rao, R. U. M. Rao, and K. Gopalan, "Surface rupture of Latur earthquake : the soil-gas helium signature," *Memoir Geological Society of India*, vol. 35, pp. 83–99, 1994.

[10] C. Y. King, "Radon monitoring for earthquake prediction in China," *Earthquake Prediction Research*, vol. 3, no. 1, pp. 47–68, 1985.

[11] C. Y. King, "Gas geochemistry applied to earthquake prediction: an overview," *Journal of Geophysical Research: Solid Earth*, vol. 91, no. B12, pp. 12269–12281, 1986.

[12] D. Thomas, "Geochemical precursors to seismic activity," *Pure and Applied Geophysics*, vol. 126, no. 2-4, pp. 241–266, 1988.

[13] H. Wakita, Y. Nakamura, and Y. Sano, "Short-term and intermediate-term geochemical precursors," *Pure and Applied Geophysics*, vol. 126, no. 2-4, pp. 267–278, 1988.

[14] G. M. Reimer, "Prediction of Central California earthquakes from soil-gas helium fluctuations," *Pure and Applied Geophysics*, vol. 122, no. 2-4, pp. 369–375, 1985.

[15] H. S. Virk, V. Walia, and N. Kumar, "Helium/radon precursory anomalies of Chamoli earthquake, Garhwal Himalaya, India," *Journal of Geodynamics*, vol. 31, no. 2, pp. 201–210, 2001.

[16] T. F. Yang, C. C. Fu, V. Walia et al., "Seismo-geochemical variations in SW Taiwan: multi-parameter automatic gas monitoring results," *Pure and Applied Geophysics*, vol. 163, no. 4, pp. 693–709, 2006.

[17] V. Walia, S. Mahajan, A. Kumar et al., "Fault delineation study using soil–gas method in the Dharamsala area, NW Himalayas, India," *Radiation Measurements*, vol. 43, pp. S337–S342, 2008.

[18] J.-P. Toutain and J. C. Baubron, "Gas geochemistry and seismotectonics: a review," *Tectonophysics*, vol. 304, no. 1-2, pp. 1–27, 1999.

[19] M. Zimmer and J. Erzinger, "On the geochemistry of gases information and drilling fluids – results from the KTB," *Scientific Drilling*, vol. 5, pp. 101–109, 1995.

[20] T. Wiersberg and J. Erzinger, "A helium isotope cross-section study through the San Andreas Fault at seismogenic depths," *Geochemistry, Geophysics, Geosystems*, vol. 8, no. 1, 2007.

[21] T. Wiersberg and J. Erzinger, "Origin and spatial distribution of gas at seismogenic depths of the San Andreas Fault from drill-mud gas analysis," *Applied Geochemistry*, vol. 23, no. 6, pp. 1675–1690, 2008.

[22] T. Wiersberg and J. Erzinger, "Chemical and isotope compositions of drilling mud gas from the San Andreas Fault Observatory at Depth (SAFOD) boreholes: implications on gas migration and the permeability structure of the San Andreas Fault," *Chemical Geology*, vol. 284, no. 1-2, pp. 148–159, 2011.

[23] Z. Gong, H. Li, C. Lao, L. Tang, and L. Luo, "Real-time drilling mud gas monitoring records seismic damage zone from the 2008 Mw 7.9 Wenchuan earthquake," *Tectonophysics*, vol. 639, pp. 109–117, 2015.

[24] S. B. Hammerschmidt, T. Wiersberg, V. B. Heuer, J. Wendt, J. Erzinger, and A. Kopf, "Real-time drilling mud gas monitoring for qualitative evaluation of hydrocarbon gas composition during deep sea drilling in the Nankai Trough Kumano Basin," *Geochemical Transactions*, vol. 15, no. 1, p. 15, 2014.

[25] T. Wiersberg, A. M. Schleicher, K. Horiguchi, M. L. Doan, N. Eguchi, and J. Erzinger, "Origin and in situ concentrations of hydrocarbons in the Kumano forearc basin from drilling mud gas monitoring during IODP NanTroSEIZE Exp. 319," *Applied Geochemistry*, vol. 61, pp. 206–216, 2015.

[26] T. Wiersberg, S. B. Hammerschmidt, S. Fuchida, A. Kopf, and J. Erzinger, "Mantle-derived fluids in the Nankai Trough Kumano forearc basin," *Progress in Earth and Planetary Science*, vol. 5, no. 1, 2018.

[27] H. K. Gupta and B. K. Rastogi, "Developments in Geotechnical Engineering," in *Dams and Earthquakes*, vol. 11, pp. 1–229, Elsevier Scientific Publishing Company, Amsterdam, Netherlands, 1976.

[28] H. K. Gupta, *Reservoir-Induced Earthquakes*, Elsevier, Amsterdam, Netherlands, 1992.

[29] H. K. Gupta, "A review of recent studies of triggered earthquakes by artificial water reservoirs with special emphasis on earthquakes in Koyna, India," *Earth-Science Reviews*, vol. 58, no. 3-4, pp. 279–310, 2002.

[30] H. K. Gupta, "Artificial water reservoir triggered earthquakes," in *Encyclopedia of Solid Earth Geophysics*, H. K. Gupta, Ed., pp. 15–24, Springer, 2011.

[31] P. Talwani, "Seismotectonics of the Koyna-Warna area, India," *Pure and Applied Geophysics*, vol. 150, no. 3-4, pp. 511–550, 1997.

[32] H. K. Gupta, C. V. Ramakrishna Rao, B. K. Rastogi, and S. C. Bhatia, "An investigation of earthquakes in Koyna region, Maharashtra for the period October 1973 through December 1976," *Bulletin of the Seismological Society of America*, vol. 70, no. 5, pp. 1838–1847, 1980.

[33] H. K. Gupta, P. Mandal, and B. K. Rastogi, "How long will triggered earthquakes at Koyna, India continue?," *Current Science*, vol. 82, no. 2, pp. 202–210, 2002.

[34] H. K. Gupta, K. Arora, N. Purnachandra Rao et al., "Investigations of continued reservoir triggered seismicity at Koyna, India," *Geological Society, London, Special Publications*, vol. 445, no. 1, pp. 151–188, 2017.

[35] S. K. Guha, P. D. Gosavi, M. M. Varma, S. P. Agarwal, J. G. Padale, and S. C. Marwadi, "Recent seismic disturbances in the Shivajisagar Lake area of the Koyna Hydroelectric Project, Maharashtra, India," Research Report Central Water and Power Research Station, Poona, India, 1968.

[36] B. K. Rastogi, R. K. Chadha, C. S. P. Sarma et al., "Seismicity at Warna reservoir (near Koyna) through 1995," *Bulletin of the Seismological Society of America*, vol. 87, no. 6, pp. 1484–1494, 1997.

[37] H. K. Gupta, "Induced seismicity hazard mitigation through water level manipulation at Koyna, India: a suggestion," *Bulletin of Seismological Society of America*, vol. 73, no. 2, pp. 679–682, 1983.

[38] S. Roy, "Scientific drilling in Koyna region, Maharashtra," *Current Science*, vol. 112, no. 11, p. 2181, 2017.

[39] N. Podugu, A. Yadav, K. Mallika, D. Goswami, and M. U. Anuradha, "Report on ICDP post–operations international workshop on "scientific deep drilling in Koyna, India"," *Journal of the Geological Society of India*, vol. 91, no. 1, pp. 120–124, 2018.

[40] GSI, "A geological report on the Koyna earthquake of 11th December, 1967," Report submitted by Officers of the Geological Survey of India, Satara District, Maharashtra State, India, 1968.

[41] H. K. Gupta, R. U. M. Rao, R. Srinivasan et al., "Anatomy of surface rupture zones of two stable continental region earthquakes, 1967 Koyna and 1993 Latur, India," *Geophysical Research Letters*, vol. 26, no. 13, pp. 1985–1988, 1999.

[42] R. V. Sathe, A. V. Padke, V. V. Peshwa, and R. K. Sukhatankar, "On the development of fissures and cracks in the region around the Koyna Nagar earthquake affected area," *Journal*

of University of Poona, Science and Technology Section, vol. 34, pp. 15–19, 1968.

[43] S. Misra, V. Bartakke, G. Athavale, V. V. Akkiraju, D. Goswami, and S. Roy, "Granite-gneiss basement below Deccan Traps in the Koyna region, western India: Outcome from scientific drilling," *Journal of the Geological Society of India*, vol. 90, no. 6, pp. 776–782, 2017.

[44] S. Niedermann, W. Bach, and J. Erzinger, "Noble gas evidence for a lower mantle component in MORBs from the southern East Pacific Rise: decoupling of helium and neon isotope systematics," *Geochimica et Cosmochimica Acta*, vol. 61, no. 13, pp. 2697–2715, 1997.

[45] T. Wiersberg, S. Süer, N. Güleç, J. Erzinger, and M. Parlaktuna, "Noble gas isotopes and the chemical composition of geothermal gases from the eastern part of the Büyük Menderes Graben (Turkey)," *Journal of Volcanology and Geothermal Research*, vol. 208, no. 3-4, pp. 112–121, 2011.

[46] H. Craig, J. E. Lupton, and Y. Horibe, "A mantle helium component in circum-Pacific volcanic gases: Hakone, the Marianas, and Mt. Lassen," in *Terrestrial Rare Gases*, E. C. Alexander and M. Ozima, Eds., pp. 3–16, Science Societies Press, Tokyo, Japan, 1978.

[47] B. A. Mamyrin and L. N. Tolstikhin, *Helium Isotopes in Nature*, Elsevier, New York, NY, USA, 1984.

[48] C. J. Ballentine and P. G. Burnard, "Production, release and transport of noble gases in the continental crust," *Reviews in Mineralogy and Geochemistry*, vol. 47, no. 1, pp. 481–538, 2002.

[49] T. J. Dunai and H. Baur, "Helium, neon, and argon systematics of the European subcontinental mantle: Implications for its geochemical evolution," *Geochimica et Cosmochimica Acta*, vol. 59, no. 13, pp. 2767–2783, 1995.

[50] A. R. Basu, P. R. Renne, D. K. DasGupta, F. Teichmann, and R. J. Poreda, "Early and late alkali igneous pulses and a high-^{3}He plume origin for the Deccan flood basalts," *Science*, vol. 261, no. 5123, pp. 902–906, 1993.

[51] D. Goswami, S. Roy, and V. V. Akkiraju, "Delineation of damage zones from 3 km downhole geophysical logs in the Koyna seismogenic zone, western India," *Journal of Geophysical Research: Solid Earth*, vol. 124, no. 6, pp. 6101–6120, 2019.

[52] S. Misra, S. Roy, V. Bartakke, G. Athavale, and H. Gupta, "Fissures and fractures in the Koyna seismogenic zone, Western India," *Journal of the Geological Society of India*, vol. 90, no. 2, pp. 131–137, 2017.

[53] H. K. Gupta, D. Shashidhar, C. R. Mahato et al., "Location of the pilot borehole for investigations of reservoir triggered seismicity at Koyna, India," *Gondwana Research*, vol. 42, pp. 133–139, 2017.

[54] D. Shashidhar, K. Mallika, C. Mahato et al., "A catalogue of earthquakes in the Koyna-Warna region, Western India (2005–2017)," *Journal of the Geological Society of India*, vol. 93, no. 1, pp. 7–24, 2019.

[55] D. Shashidhar, N. P. Rao, D. Srinagesh et al., "The 14 April 2012 Koyna earthquake of M_w 4.8: insights into active tectonics of the Koyna region," *Journal of Seismology*, vol. 17, no. 4, pp. 1345–1353, 2013.

[56] D. Shashidhar, K. Mallika, C. R. Mahato, B. S. Maity, and H. V. S. Satyanarayana, "Recent seismicity patterns and microearthquake activity on an active intraplate fault system at Koyna-Warna, western India," *Journal of the Geological Society of India*, vol. 90, no. 6, pp. 798–801, 2017.

[57] Y. J. Bhaskar Rao, B. Sreenivas, T. Vijaya Kumar, N. Khadke, A. Kesava Krishna, and E. V. S. S. K. Babu, "Evidence for Neoarchean Basement for the Deccan volcanic flows around Koyna-Warna region, Western India: zircon U-Pb age and Hf-isotopic results," *Journal of the Geological Society of India*, vol. 90, no. 6, pp. 752–760, 2017.

[58] T. Torgersen, "Continental degassing flux of ^{4}He and its variability," *Geochemistry, Geophysics, Geosystems*, vol. 11, no. 6, 2010.